Lens

Analyzing Effect of Waterclefts on Visual Functions Via Optical Simulations

Yusuke Seki,[1,2] Takushi Kawamorita,[3] Naoki Yamamoto,[4,5] Takashi Tanigawa,[6] Norihiro Mita,[2] Natsuko Hatsusaka,[4] Eri Kubo,[4] and Hiroshi Sasaki[4]

[1]Division of Vision Research, Kanazawa Medical University Graduate School of Medical Science, Kahoku, Ishikawa, Japan
[2]Medical Technology Division, Kanazawa Medical University Hospital, Kahoku, Ishikawa, Japan
[3]Orthoptics and Visual Science Course, School of Allied Health Sciences, Kitasato University, Sagamihara, Kanagawa, Japan
[4]Department of Ophthalmology, Kanazawa Medical University, Kahoku, Ishikawa, Japan
[5]Center for Clinical Trial and Research Support, Research Promotion and Support Headquarters, Fujita Health University, Toyoake, Aichi, Japan
[6]Engineering Department, CAE Division II, CAE BU., Cybernet Systems Co., Ltd., Chiyoda-ku, Tokyo, Japan

PURPOSE. To investigate the impact of the size and location of waterclefts (WC), which are one of several cataract subtypes, on visual function by optical simulation analysis.

METHODS. An optical simulation software (CODE V) was used to develop a schematic eye model and several sizes of WC central and peripheral types that were located below the anterior and posterior subcapsules of the crystalline lens, and analyses of refraction, higher-order aberrations (HOA), and the modulation transfer function (MTF) were performed.

RESULTS. An increase in the WC size increased the refraction and HOA and decreased the MTF. The impact of the WC below the posterior subcapsule on the visual function was more enhanced than that below the anterior subcapsule. Large WC demonstrated a remarkable hyperopic shift in refractive power as well as an increase in HOA. The MTF decreased slightly with increasing WC size at a spatial frequency of 20 cycles/mm, and it decreased remarkably at 60 cycles/mm.

CONCLUSIONS. The impact on the visual function increased with increasing WC size. It was revealed that eyes with WC below the posterior subcapsule are more hyperopic than those with WC below the anterior subcapsule, and the former have a higher HOA and lower MTF than the latter.

Keywords: waterclefts, visual function, refraction, higher-order aberration, modulation transfer function

A study on the global burden of diseases[1] reported that cataract was the leading cause of blindness in 2020; a total of 15.2 million cataract patients aged 50 and above accounted for 45.2% of the blind patients. Owing to an increase in life expectancy and a decrease in the birth rate, the global population is rapidly aging. The number of people aged 65 and above is estimated to become more than 1.5 billion in 2050, which is twice the current number.[2] Aging is likely to increase the number of cataract patients in the future.

Three main types of cataracts, namely, cortical, nuclear, and posterior subcapsular cataracts, are globally recognized and diagnosed clinically. This study focuses on a subtype of cataracts, called waterclefts (WC), which typically occur in the anterior superficial cortical zone or in both anterior/posterior cortices (52% and 47%, respectively).[3] They are also found in the posterior cortical zone, but are smaller and are found less frequently than those found in the anterior cortical zone. Sutural cataracts, similar to WC, are opacities that occur in the Y-suture in the nucleus or cortex

of the lens. In contrast, WC are caused by the separation of the lens cortex along Y-sutures in the superficial layers of the crystalline lens; this phenomenon is sometimes called lamella separation. Their subsequent formation as an axial type of cortical cataracts may be called sutural cataracts in the broad sense.[4] WC have a prevalence of 4.7% to 41.4% depending on age, race, climate, and cataract classification (Table 1). Patients with WC exhibit a reduction in their visual function clinically, such as hyperopia owing to a reduction in the refractive power of the crystalline lens and a significantly greater total higher-order aberration (HOA) than those whose eyes have transparent lenses (Table 2).[5,6] We have previously studied the influence of subsurface nano-glistening on visual function in eyes through optical simulations utilizing an acrylic intraocular lens[7]; however, no study has analyzed WC while differentiating between the anterior and posterior subcapsules in optical simulations.

Artal et al.[8] reviewed the publications on the optics of the human eye and schematic eye models that have contributed to the research on the visual function of the human eye since

Investigative Ophthalmology & Visual Science

TABLE 1. Reports on the Prevalence of WC

Author	Year of Report	Eye Study	Subjects	Cataract Classification	Prevalence of WC (95% CI)
Brown N.A.P.[28]	1989	–	20 patients (M: 8, F: 12, mean age 75.5 y)	CCRUO	17%
Deane J.S.[29]	1997	Melton Eye Study	1090 eyes of 560 subjects (M: 265, F: 295, 55–74 y)	OCCCGS	17% (14–21)
Frost N.A.[30]	2002	Somerset and Avon Eye Study	From 902 subjects (M: 431, F: 471, mean 68 (55–95) y), 1473 eyes of 839 subjects were analyzed	OCCCGS	23.7%
Qu J.[31]	2005	Monzen Eye Study	442 eyes of 225 subjects (M: 101, F: 124, mean 67.8 $\pm$ 7.0 (55–85) y)	Existence or absence	41.4%
Miyashita H.[10]	2019	–	1801 subjects (M: 700, F: 1101) of $\geq$ 40 y	KMUCCGS	Sanya = 4.7% (2.7–6.6)
					Taiyuan = 7.2% (5.2–9.2)
					Taichung = 11.9% (9.5–14.3)

95% CI: 95% confidence interval; M: male; F: female; CCRUO: Clinical Cataract Research Unit at Oxford; OCCCGS: Oxford Clinical Cataract Classification and Grading System; KMUCCGS: Kanazawa Medical University Cataract Classification and Grading System.

TABLE 2. Reports on the Visual Functions of Eyes With WC in Comparison With Those of the Control

Author	Year of Report	Eye Study	Subjects	Cataract Classification	Significant Parameters in Visual Function Compared With Control ($P < 0.05$)
Qu J.[5]	2010	Reykjavik Eye Study	30 WC eyes (M: 13, F: 17, 72.1 $\pm$ 4.5 y),	Existence or absence	CDVA, total RMS; HOAs, trefoil, internal eye RMS; HOAs, coma, trefoil
			194 control eyes (M: 97, F: 97, 66.8 $\pm$ 4.5 y)		
Tanimura N.[6]	2019	Monzen Eye Study and KMUH	70 WC eyes (mean 68.1 $\pm$ 6.9 y); 27 WC-1 eyes, 20 WC-2 eyes, 23 WC-3 eyes 77 control eyes (mean 66.7 $\pm$ 5.0 y)	KMUCCGS	CDVA, 100% and 25% CVA, Straylight, cylinder, LP

M: male; F: female; y: years; CDVA: corrected distance visual acuity; RMS: root mean square; KMUH: Kanazawa Medical University Hospital; WC-1, 2, and 3: parameters of WC types (see[7]); KMUCCGS: Kanazawa Medical University Cataract Classification and Grading System; CVA: contrast visual acuity; LP: lens power.

the time of Galileo, such as Young (1801), Moser (1844), Listing (1851), Helmholtz (1855), Tscherning (1900), Gullstrand (1909), Emsley (1952), Smirnov (1961), Hage-Berny (1973), Millodot–Sivak (1979), Le Grand (1980), Kooijman (1983), Navarro (1985), and Liou and Brennan (1997). Although it is challenging to accurately predict the visual function of eyes with cataracts via optical simulations, it is essential to use the aforementioned eye model for a more accurate evaluation of the visual function. Because the refractive index distribution in the lens varies depending on aging and opacity type, it is difficult to create an accurate eye model; however, WC is space created by cleavage of the Y-suture, its internal structure is filled with liquid components, and the refractive index is close to that of the anterior chamber.[6,9] Thus, compared with other opacity types, the use of optical simulation can enable accurate prediction of the visual function of eyes with WC.

This study investigated the refraction, HOA, and modulation transfer function (MTF) in eyes with WC through an optical simulation analysis after locating various sizes of WC

below the anterior and posterior subcapsules of the crystalline lens.

METHODS

Typical Types and Locations of WC

Figure 1 shows the typical types and locations of WC in crystalline lenses. The case images of WC were obtained from Monzen Eye Study, a longitudinal epidemiological survey (2013–2016) involving general residents in Monzen-machi, Ishikawa Prefecture, Japan, and from the eyes of patients with WC at the Kanazawa Medical University Hospital (2013–2017).[6] They were classified according to the Kanazawa Medical University Cataract Classification and Grading System,[10] by slit-lamp microscopy with maximum pupil dilatation and the lens images acquired by an anterior eye segment analysis system (EAS-1000, NIDEK Co., Ltd., Tokyo, Japan) and anterior segment optical coherence tomography (CASIA2, Tomey Corporation, Aichi, Japan).
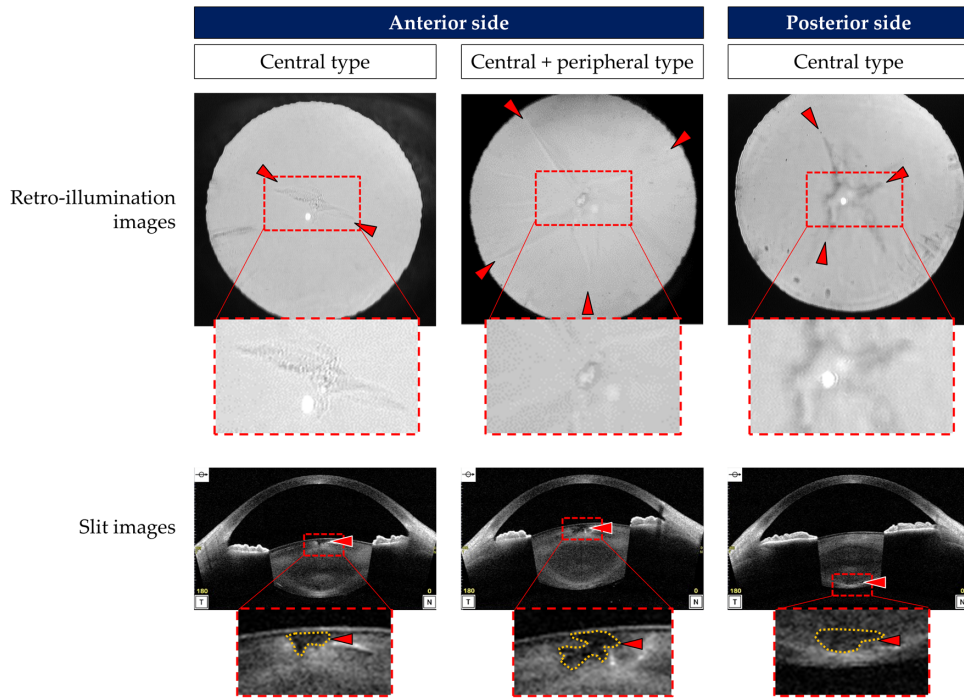
FIGURE 1. Typical types and locations of WC. Cases images of central or central + peripheral types on anterior side and central type on posterior side were obtained from 54-year female, 65-year female, and 54-year female, respectively.

The study was approved by the Institutional Review Board of Kanazawa Medical University (protocol number I375) and was conducted in accordance with the provisions of the Declaration of Helsinki. Informed written consent was obtained from all participants.

Optical Design Software for Analysis

CODE V (Synopsys Inc., Mountain View, CA), a commercial optical design software, was used to perform the optical simulations. Reliable imaging optics were designed, optimized, and fabricated using this software. A previous report on MTF measuring instruments has established the accuracy of CODE V, which stated that the deviations between actual measurements and CODE V predictions are within ±4%.[11]

Schematic Eye Model

A schematic eye model modified by Navarro[12,13] and Liou and Brennan[14] was used to evaluate the visual function in eyes with WC in this study. The structural parameters of the schematic eye model used in the current study and the ones adopted by Navarro and by Liou and Brennan are listed in Table 3.

TABLE 3. Structural Parameters of the Schematic Eye Models

		Schematic Eye Model in This Study	Navarro et al.[12,13]	Liou and Brennan[14]
Radius of curvature (mm)				
Cornea	Anterior	**7.72**	**7.72**	7.77
	Posterior	**6.50**	**6.50**	6.40
Lens	Anterior	**10.2**	**10.2**	
	Posterior	**−6.0**	**−6.0**	
Asphericity				
Cornea	Anterior	**−0.18**	−0.26	**−0.18**
	Posterior	**−0.60**	0	**−0.60**
Thickness (mm)				
Cornea		**0.55**	**0.55**	0.50
Lens		**4.0**	**4.0**	4.02
Refractive index				
Cornea		**1.376**	1.367	**1.376**
Aqueous		**1.337**	1.3374	1.336
Lens		**1.42**	**1.42**	–
Vitreous		**1.336**	**1.336**	**1.336**

The bold values represent the schematic eye model used in this study.
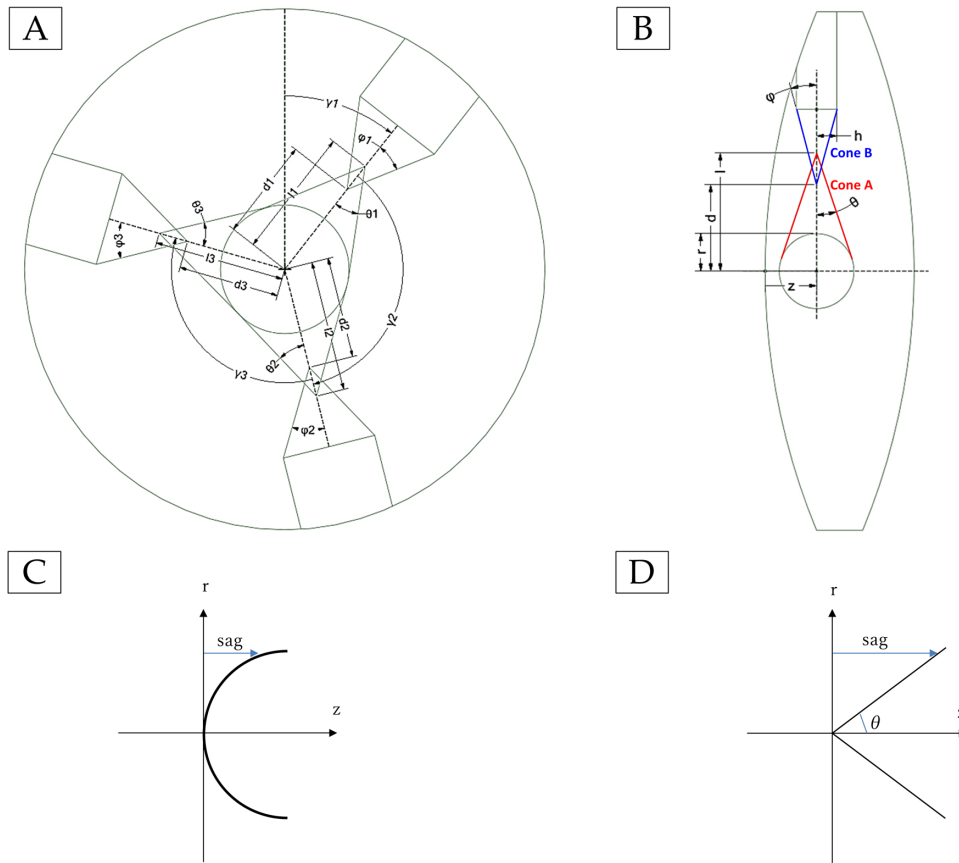
FIGURE 2. WC shape definition created by CODE V macro. (**A**) X–Y plan view of WC ($n = 3$), (**B**) Y–Z plan view of WC ($n = 1$, $\gamma = 0$), (**C**) spherical surface, and (**D**) conical surface.

CODE V Macro Creation to Model WC in the Specified Lens

We created the macro that models the shape shown in Figures 2A and 2B as nonsequential surfaces in the specified lens model. Various types and sizes of WC can be created by specifying the parameters shown below.

Cone A: Cones with vertices facing the outside of the lens

Cone B: Cones with vertices facing the inside of the lens

d1, d2, d3: Distance from the center of the sphere to the apex of Cone B

h: Radius of the base of Cone B

l1, l2, l3: Distance from the center of the sphere to the apex of Cone A

n: Number of the conical central axis

r: Radius of the central sphere

z: Distance from the surface apex on the front of the lens to the center of the sphere

$\gamma 1$: Rotation angle from the y-axis of the lens coordinate system to the central axis of the first cone

$\gamma 2$, $\gamma 3$: Rotation angle between the central axes of adjacent cones

$\theta 1$, $\theta 2$, $\theta 3$: Apex angle of Cone A

$\varphi 1$, $\varphi 2$, $\varphi 3$: Apex angle of Cone B

Formula of the WC Spherical Surface

To simulate the spherical surface of WC (Fig. 2C), the following formula was used. Because the formula defines a hemi-sphere, the sphere is composed of two surfaces.

$$z = \frac{cr^2}{1 + \sqrt{1 - c^2 r^2}},$$

where:

z: Sag of the surface parallel to the z-axis

c: Curvature at the pole of the surface

$$c = \frac{1}{radius\ of\ curvature*},$$

where:

*Radius of curvature is specified by the radius of the central sphere.

r: Radial distance from the z-axis.

Formula of the WC Conical Surface

The following formula was used to simulate the conical surface of WC (Fig. 2D).

$$z = \frac{cr^2}{1 + \sqrt{1 - (1 + k) c^2 r^2}},$$

where:

z: Sag of the surface parallel to the z-axis
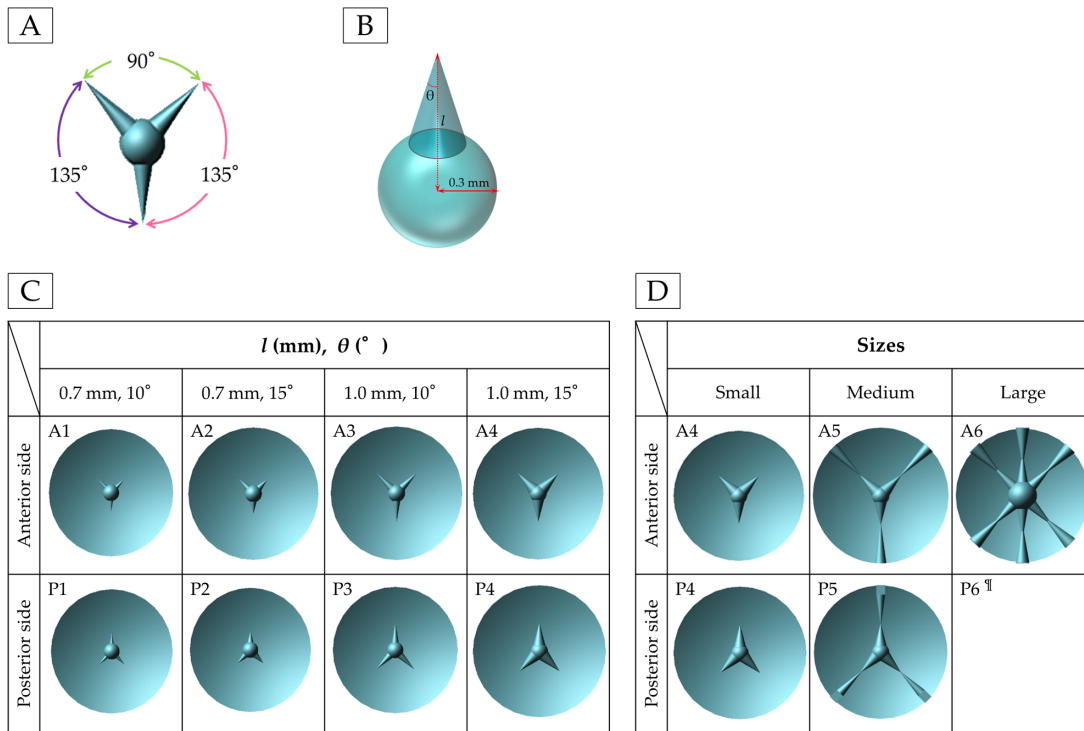
FIGURE 3. WC central types created using CODE V. (**A**) Schematic of the WC shape, (**B**) WC shape setting of the center sphere and cone, (**C**) WC central types, (**D**) WC central or central + peripheral types. A: anterior; P: posterior; ¶: The large size on the posterior side displayed an error upon the execution of CODE V.

c: Curvature at the pole of the surface, which is used as a fixed value

$$c = 10^6,$$

where:

r: Radial distance from the z-axis

k: Conic constant

$$k = -\left(1 + \tan^2\theta\right),$$

where:

θ: Apex angle (half angle) of the cone

Simulation Values Analyzed Using CODE V

The ocular refractive power, ocular total HOA, ocular spherical aberration, and MTF (spatial frequency: 20, 60, 100, and 200 cycles/mm) of several types of WC were analyzed using CODE V. The refractive power and MTF were analyzed using a 3.0-mm diameter pupil in the simulation, which is equal to the value assumed for daily vision. Similarly, HOA was analyzed using a 6.0-mm diameter pupil, which is usually measured under mydriasis clinically. The wavelength of the light ray was 587.56 nm.

First Simulation: Shape Setting of the WC Central Types

The schematics of WC shapes for the first simulation were developed from a retroillumination image of WC. The angles of the three cones extending from the central sphere that were used to create the schematics were 90°, 135°, and 135° (Fig. 3A); the first angle (90°) corresponds with twice $\gamma 1$ in Figure 2, whereas the other two angles (135°) are $\gamma 2$ and $\gamma 3$. The radius of the central sphere was 0.3 mm, the distance between the center of the sphere and the apex of the cone was "l," the apex angle of the cone was "θ," and the WC material was set as water (Fig. 3B).

Four sizes of WC samples were generated during the first simulation, including a Y-shaped WC 0.5 mm below the anterior subcapsule and an inverted Y-shaped WC 0.5 mm below the posterior subcapsule (Fig. 3C), because Y-sutures are observed inversely in the anterior and posterior subcapsules of the actual human crystalline lens.[15] l and θ were set as (0.7 mm and 10°) or (1.0 mm and 15°), to eliminate simulation errors in the WC generation program, which occur if the bottoms of adjacent cones overlap or the WC pop out of the crystalline lens. The simulation excluding the WC shape was defined as the control.

Second Simulation: Shape Settings of the WC Central or Central + Peripheral Types

Three sizes of the WC central or central and peripheral types were generated during the second simulation, including a Y-shaped WC 0.5 mm below the anterior subcapsule and an inverted Y-shaped WC 0.5 mm below the posterior subcapsule (Fig. 3D).

WC central types (A4, P4) with 1.0 mm (l) and 15° (θ) were defined as small. The WC peripheral type with a medium size (A5, P5) extended to the apices of the three cones of the small type. The number of cones in the large size variant (A6, P6) was doubled to six to assess the effect
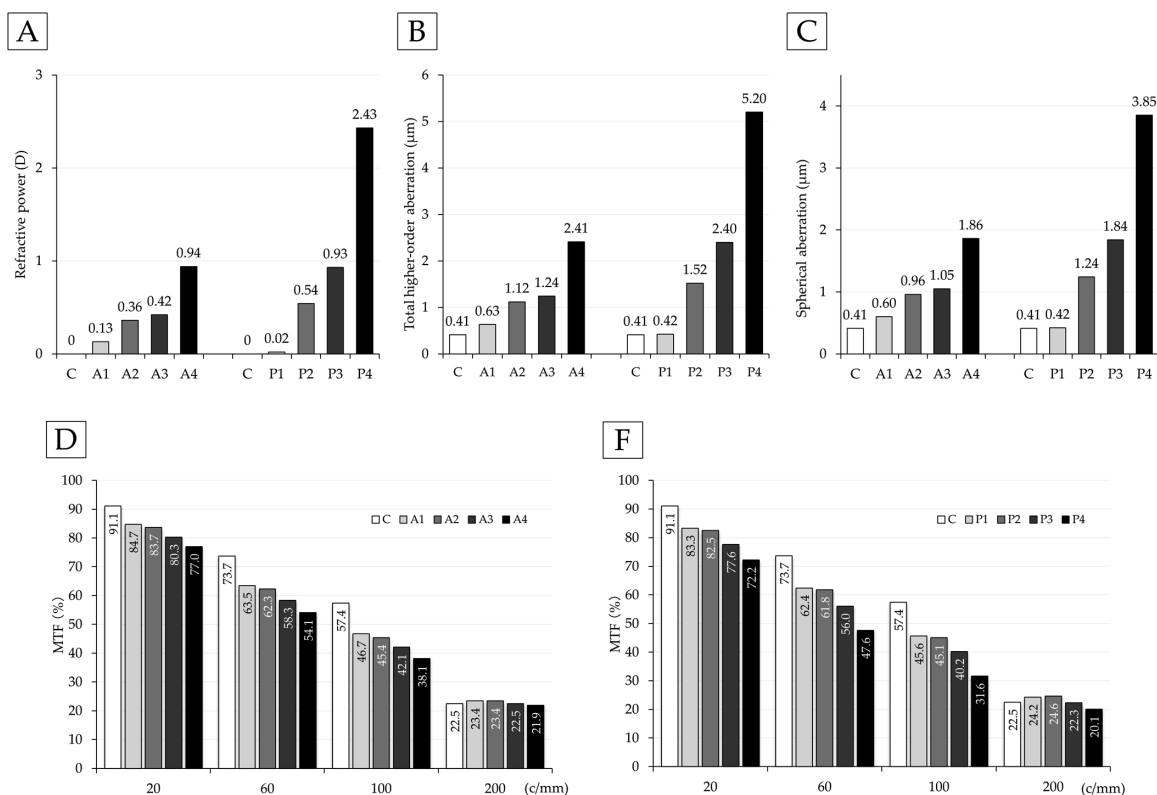
FIGURE 4. (**A**) Refractive power, (**B**) total HOA, and (**C**) spherical aberrations of different WC central types. MTFs for different WC central types on the (**D**) anterior and (**E**) posterior sides. D: diopter; A: anterior; P: posterior; C: control; c/mm: cycles/mm.

of the number of cones. The radius of the central sphere was set to 0.5 mm to eliminate simulation errors if the bottoms of adjacent cones overlap. However, an error prevented the analysis of the posterior side (P6), indicating that the WC could protrude from the posterior subcapsule because the curvature of the posterior subcapsule was steeper than that of the anterior subcapsule.

RESULTS

First Simulation: Comparison Among the Visual Functions of the WC Central Types

Figure 4A presents ocular refractive power by size of the WC central types. The refractive power for the control was set to 0. The refractive power increases hyperopically on the anterior and posterior sides with increasing WC size. The influence of the posterior WC on refractive power showed more hyperopia than that of the anterior WC.

Similar to the refractive power variation, the total HOA and spherical aberration increased with increasing WC size (Figs. 4B, 4C). Despite a constant WC size, the increment in the number of aberrations on the posterior side was greater than that on the anterior side, except for a minor difference in the predicted results of the WC with 0.7 mm (*l*) and 10° (*θ*) (A1, P1).

The MTFs on the anterior and posterior sides decreased with increasing WC size at spatial frequencies ranging from 20 to 100 cycles/mm (Figs. 4D, 4E). The rate of reduction of the MTF was slightly higher on the posterior side than on the anterior side for a constant WC size at spatial frequencies ranging from 20 to 100 cycles/mm. The MTF remained

constant across grades of opacity on the anterior and posterior sides at a spatial frequency of 200 cycles/mm.

A comparison with the MTF curves in Figure 5 indicated that the decrease in the MTF on the posterior side was slightly greater than that on the anterior side for a constant WC size. The reduction in the MTF values was maximum at spatial frequencies ranging from 80 to 120 cycles/mm.

Second Simulation: Comparisons Between the Visual Functions of WC Central or Central + Peripheral Types

Figure 6A compares the refractive powers of different WC central or central and peripheral types. The refractive power increased hyperopically on the anterior and posterior sides with increasing WC size. For a constant WC size, P5 was approximately 2.6 times more hyperopic than A5. Severe hyperopic shifting was observed in A6, which is the large size of WC. An error occurred while calculating the values for P6 in the software.

Similar to the variation of the refractive power, the total HOA and spherical aberration increased on the anterior and posterior sides with increasing WC size (Figs. 6B, 6C). The aberrations on the posterior side were greater than those on the anterior side for a constant WC size.

The MTFs of different WC central or central + peripheral types decreased with increasing WC size on both the anterior and posterior sides (Figs. 6D, 6E). Additionally, the decrease in the MTF on the posterior side was relatively larger than that on the anterior side. Compared with the WC central type, the MTF of WC central and peripheral type
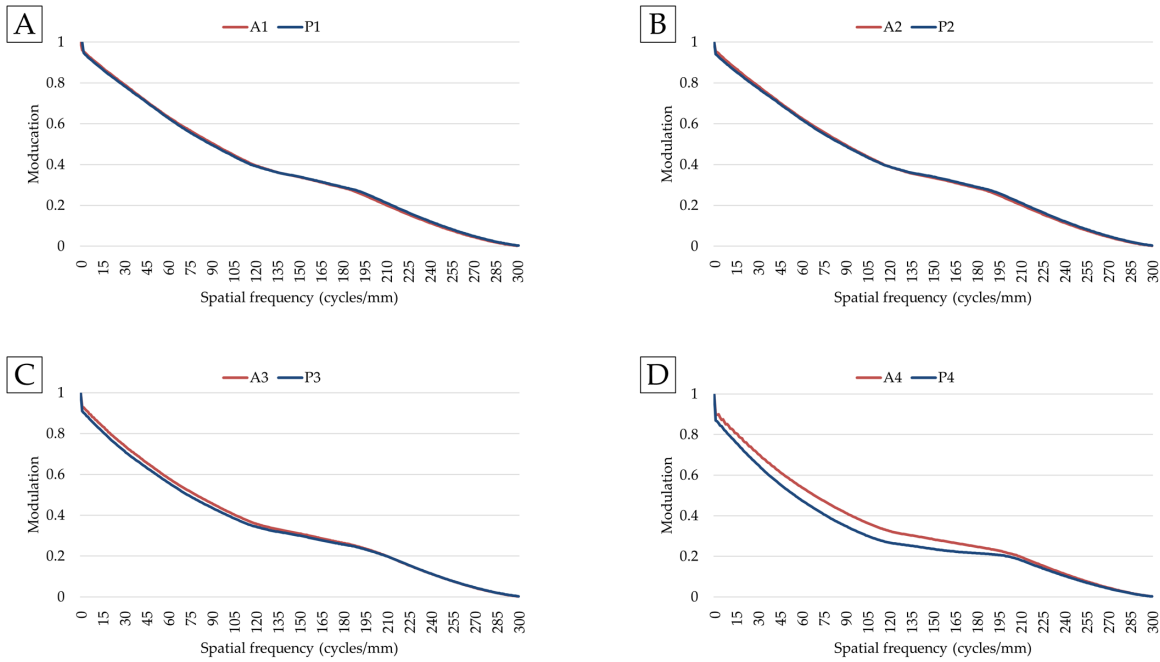
FIGURE 5. WC sizes and MTF curves of WC central types: (**A**) A1 and P1: l = 0.7 mm; $\theta = 10°$; (**B**) A2 and P2: l = 0.7 mm; $\theta = 15°$; (**C**) A3 and P3: l = 1.0 mm, $\theta = 10°$; (**D**) A4 and P4: l = 1.0 mm; $\theta = 15°$. A: anterior side; P: posterior side.
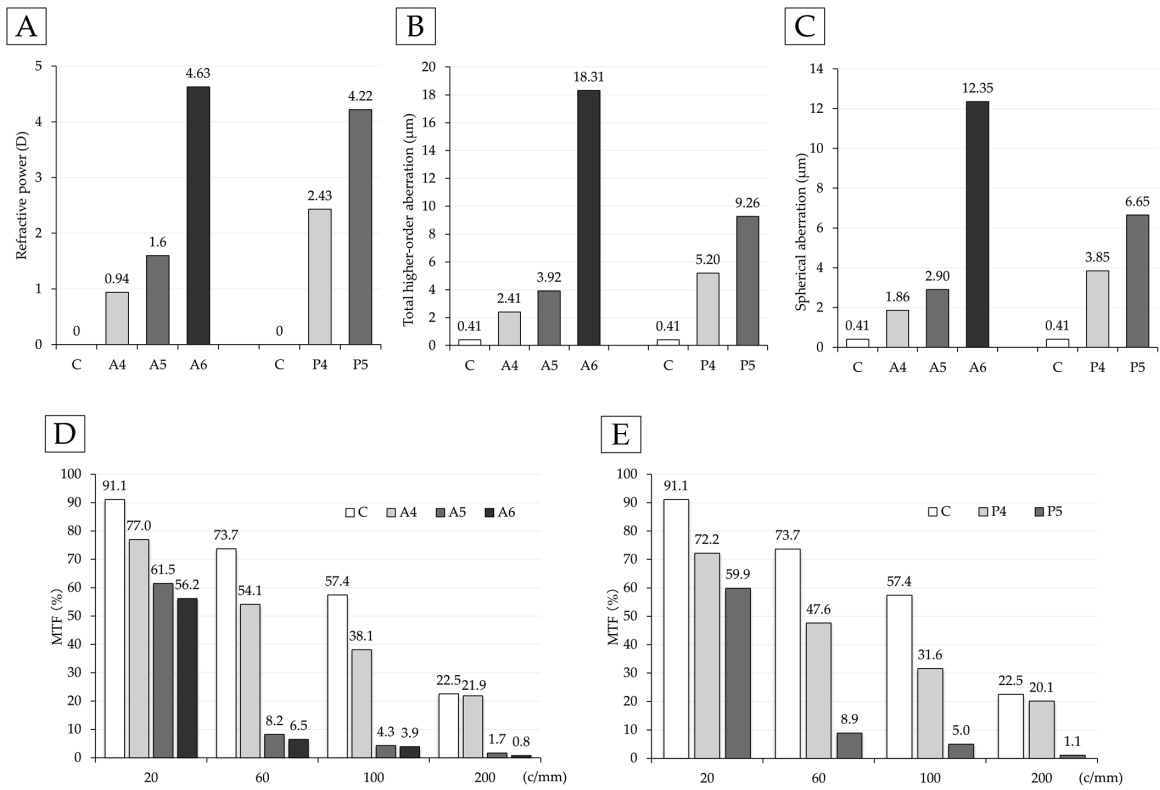
FIGURE 6. (**A**) Refractive power, (**B**) total HOA, and (**C**) spherical aberrations of different WC central or central + peripheral types. MTFs for different WC central or central + peripheral types at the (**D**) anterior and (**E**) posterior sides. D: diopter; A: anterior; P: posterior; C: control; c/mm: cycles/mm.
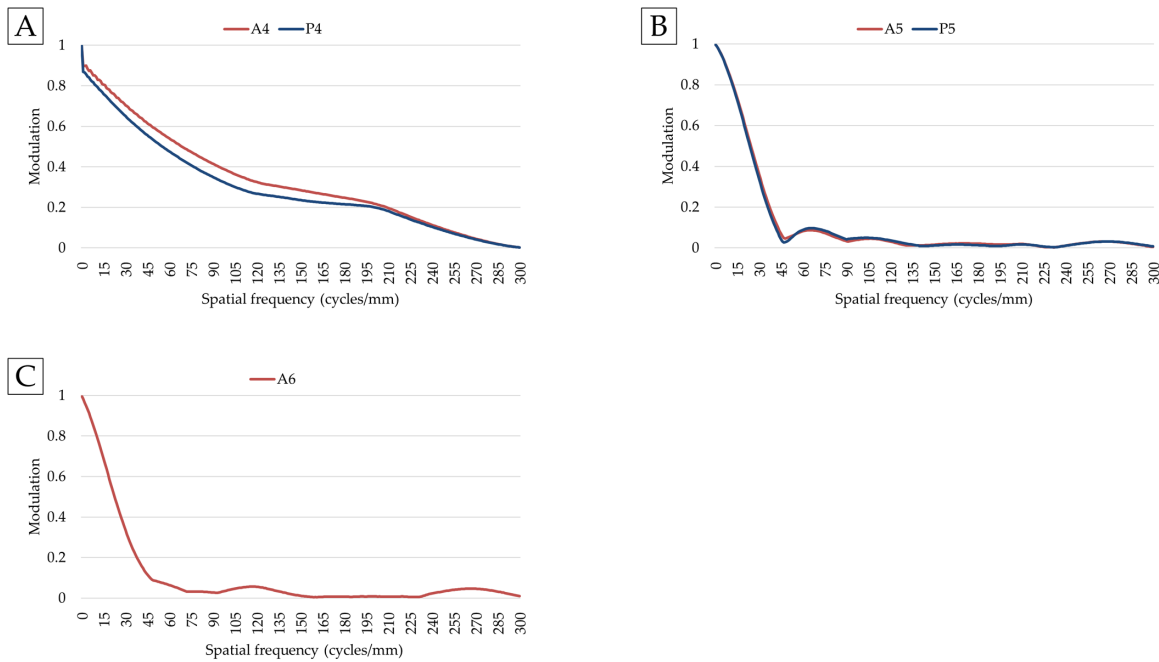
FIGURE 7. WC sizes and MTF curves of WC central or central + peripheral types: (**A**) A4 and P4: small size, (**B**) A5 and P5: medium size, (**C**) A6: large size. A: anterior side; P: posterior side.

decreased remarkably, especially at a spatial frequency of 60 cycles/mm.

A comparison with the MTF curves in Figure 7 indicated that although the MTFs for the small size variant showed a slight decrease at the intermediate spatial frequency, the MTFs for the medium and large size variant decreased significantly at most of the spatial frequencies, except at the low frequency.

DISCUSSION

This study is the first to investigate the influence of the size and location of the WC on refraction, HOA, and MTF through an optional simulation analysis.

The eye models proposed by Gullstrand[16,17] and LeGrand[18,19] have been widely accepted as typical optical designs in the past.[20] However, eye models have been reported that are more similar than previous models to the actual eyeball because of the ability of new models to account for the asphericity of the refractive surface and the refractive index structure of the lens. The Gullstrand eye model, which was based on physiological findings, is used to analyze the physiological shape of the eye and to optically examine the focal length or image formation. Because the corneal and lenticular surfaces in this model are spherical and the refractive index of the lens is uniform, this eye model was not suitable for the current study, which simulates HOA. The Liou–Brennan eye model,[14] which was adopted in our previous study[7] because of suitability for calculating the accommodation and off-axis aberration, was not fully adopted in the current study because of the refractive index structure that was obtained when the WC was placed below the anterior or posterior subcapsule of the lens. The Navarro eye model,[12,13] which is used as a standard human eye model in the field of eye optics, accounts for the asphericity of the anterior surface of the cornea,

holds the uniform lenticular refraction, and reflects aberration measurements, such as the ocular off-axis aberration, thereby accurately simulating the WC in the lens. Thus, this study used the schematic eye model modified by Navarro and Liou and Brennan to evaluate the refractive power, HOA, and MTF in eyes with WC.

These optical simulations indicated that hyperopia progressed with increasing WC size, and the total HOA and spherical aberration also increased, which is consistent with our previous studies of clinical cases.[5,6] Tanimura et al.[6] reported an 0.5-diopter (D) difference of refractive power of the crystalline lens between the control (21.8 D) and WC central type (22.3 D), which is comparable to the results (0.13–0.42 D) in this simulation, having sizes similar to those of A1, A2, and A3 in this study and being located near the anterior subcapsule. Tanimura et al. further reported that the refractive power of the lens decreased by approximately 2 D in the central and peripheral type of WC, which is equivalent to about a 1.3-D hyperopic shift when converted to the refractive power of the eyeball; because A5 (central and peripheral type) had 1.6 D hyperopically in this eye model, it is almost consistent with Tanimura's report. In contrast, clinically observed WC in the posterior subcapsule are typically only small in size, similar to P1 and P2 in this study. Because severe hyperopia was predicted in P3 and above in this simulation, it is necessary to verify hyperopia in clinical cases in the future. Regarding aberrations, Tanimura et al.[6] reported that the ocular total HOA (6.0 mm diameter pupil) increased significantly to 0.725 μm and 0.853 μm in eyes with WC central and central and peripheral types, respectively, compared with those with a transparent lens (0.564 μm). In this study, the total HOA increased with increasing WC sizes, and the amount of increase was larger than that in the clinical cases; thus, it is necessary to improve the schematic eye model to match clinical values more closely in the future. Using this model, it was revealed that
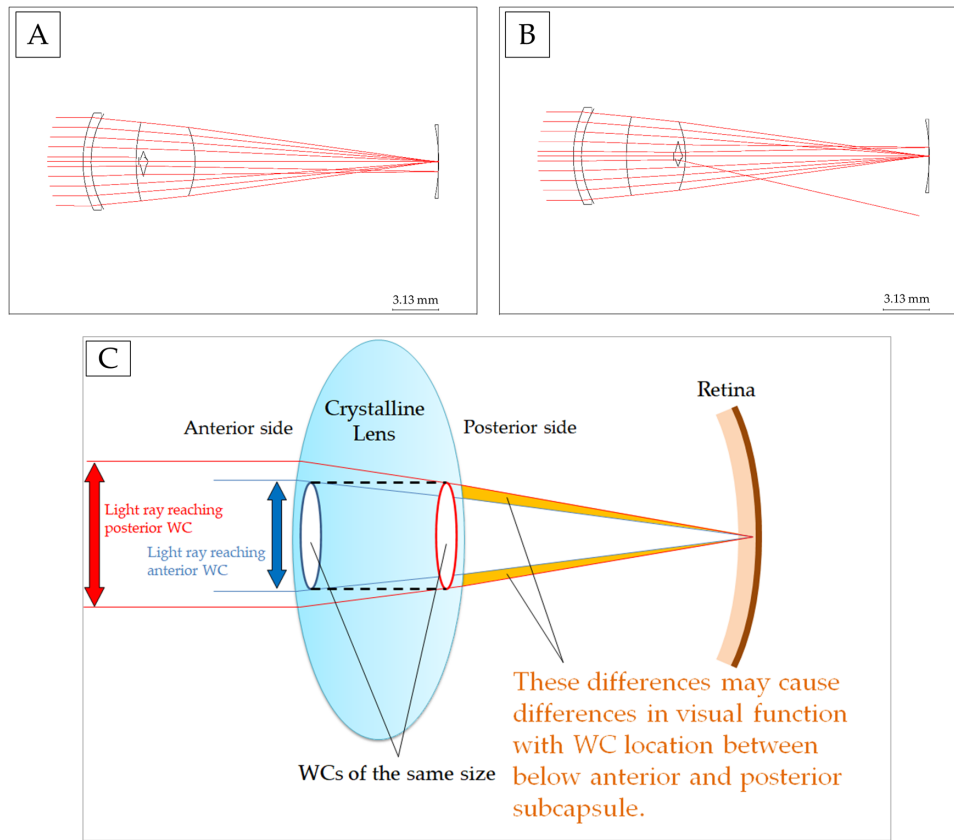
FIGURE 8. Light ray loci passing through (**A**) a Y-shaped WC 0.5 mm below the anterior subcapsule of the crystalline lens and (**B**) an inverted Y-shaped WC 0.5 mm below the posterior subcapsule of the crystalline lens. (**C**) Hypothesis for the reduction in the visual function.

the MTF in eyes with WC decreased with increasing size and HOA. The decrease in the MTF in the human eye manifests as a decrease in contrast sensitivity.[21–23] We had previously reported that the contrast visual acuity decreased with increasing size of the WC central type,[6] which is consistent with the results of this simulation.

It was observed that the refractive power shifted hyperopically in the eyes wherein the WC was located below the anterior subcapsule, and this was further enhanced when the WC was located below the posterior subcapsule. In addition, the ocular total HOA and spherical aberration also increased, and HOA of the eyes with the WC located below the posterior subcapsule increased compared with that of eyes with WC located below the anterior subcapsule. There was no difference between the MTFs of the eyes with the WC located below the anterior and posterior subcapsule at higher spatial frequencies, but the MTF of the eyes with the WC located below the posterior subcapsule was lower than that of eyes with WC located below the anterior subcapsule at spatial frequencies of less than or equal to 100 cycles/mm. The reason for the greater influence of the posterior WC than the anterior WC may be as follows: if the light ray loci passing through the cornea, aqueous, lens, and vitreous to the retina were simulated by models wherein the WC was located below the anterior and posterior subcapsules, the light rays would converge near the center of the retina when WC were located below the anterior subcapsule. This is in contrast with the light rays in the model where the WC was located below the posterior subcapsule (Figs. 8A, 8B). In addition, it is presumed that the hyperopia, increased aber-

rations, and decreased MTF may cause more refracted light rays to pass through the WC below the posterior subcapsule than those below the anterior subcapsule (Fig. 8C).

The WC below the anterior subcapsule can be easily observed using a slit-lamp microscope; however, those below the posterior subcapsule are often overlooked because of the influence of other types with varying opacities. These optical simulations indicate that the posterior subcapsular WC influences the visual function more strongly than the anterior subcapsular WC. Thus, it is important to conduct a reliable slit-lamp examination for the posterior subcapsular WC. In addition, the introduction of several IOLs in recent years, such as toric, multifocal, expanded depth-of-field, and refractive segmented multifocal IOLs, has ensured that more detailed patient needs are catered to than ever before. Thus, it is important to determine the surgical indications that help understand the effects of different types of cataracts, that is, not only the three main types (cortical, nuclear, and posterior subcapsular cataracts) but also the subtypes of cataracts (WC, retrodots, blue dots, fiber folds, etc.), on visual function.

This study has several limitations. First, the refractive index of the lens of the schematic eye model is constant. Thus, refraction only occurs at the interface, following which the light rays travel in a straight path. However, actual human eyes have crystalline lens with a nonuniform refractive distribution. The refractive index depends on the part of the crystalline lens being analyzed.[12,24–27] Second, WC were analyzed using a combination of conical structures in this study, whereas they have a variety of shapes; for

example, some clinically resemble cylinders rather than cones. In addition, the program used to generate the WC through CODE V in this study generated an error on increasing the WC size above a certain level. Further, it is impossible to generate the WC below the anterior and posterior subcapsule simultaneously or only in the peripheral region of the lens. Future studies can improve the program and perform simulations with WC shapes that are more identical to clinical cases than the current ones.

In conclusion, this study revealed the influence of WC on visual function. The increasing size of WC increases its impact on the visual function, eyes with WC below the posterior subcapsule are more hyperopic than those with WC below the anterior subcapsule, and the former has a higher HOA and lower MTF than those of the latter. Further investigations using this optical simulation technique may be highly beneficial in assessing the visual functions of other opacity types and aid ophthalmologists in determining surgical indications.

References

1. GBD 2019 (Blindness and Vision Impairment Collaborators and Vision Loss Expert Group of the Global Burden of Disease Study). Causes of blindness and vision impairment in 2020 and trends over 30 years, and prevalence of avoidable blindness in relation to VISION 2020: the Right to Sight: an analysis for the Global Burden of Disease Study. _Lancet Global Health_. 2021;9:e144–e160.

2. United Nations Department of Economic and Social Affairs, Population Division. World Population Ageing 2020 Highlights: Living arrangements of older persons (ST/ESA/SER.A/451). 2020. Available at: https://www.un.org/development/desa/pd/sites/www.un.org.development.desa.pd/files/undesa_pd-2020_world_population_ageing_highlights.pdf.

3. Durant JS, Frost NA, Trivella M, Sparrow JM. Risk factors for cataract subtypes waterclefts and retrodots: two case-control studies. _Eye_. 2006;20:1254–1267.

4. Yang Z, Li Q, Ma Z, Guo Y, Zhu S, Ma X. A G–>T splice site mutation of CRYBA1/A3 associated with autosomal dominant suture cataracts in a Chinese family. _Mol Vis_. 2011;17:2065–2071.

5. Qu J, Sasaki H, Sakamoto Y, Kawakami Y, Sasaki K, Jonasson F. Higher-order ocular aberrations caused by crystalline lens waterclefts. _J Cataract Refract Surg_. 2010;36:799–805.

6. Tanimura N, Hatsusaka N, Miyashita H, et al. Visual function and functional decline in patients with waterclefts. _Invest Ophthalmol Vis Sci_. 2019;60:3652–3658.

7. Takahashi Y, Kawamorita T, Mita N, et al. Optical simulation for subsurface nanoglistening. _J Cataract Refract Surg_. 2015;41:193–198.

8. Artal P, Tabernero J. Optics of human eye: 400 years of exploration from Galileo's time. _Appl Opt_. 2010;49:D123–130.

9. Uozato H. Optical properties of the eye and vision correction. _Kogaku: Japanese journal of optics_. 2002;31:2–8.

10. Miyashita H, Hatsusaka N, Shibuya E, et al. Association between ultraviolet radiation exposure dose and cataract in Han people living in China and Taiwan: a cross-sectional study. _PLoS One_. 2019;14:e0215338.

11. Cabib D, Rahav A, Barak T. Broad-band optical test bench (OPTISHOP) to measure MTF and transmittance of visible and IR optical components. _Proceedings of SPIE - The International Society for Optical Engineering – Infrared Imaging Systems: Design, Analysis, Modeling, and Testing XVIII_. 2007;6543:654311.

12. Navarro R, Santamaria J, Bescos J. Accommodation-dependent model of the human eye with aspherics. _J Opt Soc Am A_. 1985;2:1273–1281.

13. Navarro R. The optical design of the human eye: a critical review. _J Optom_. 2009;2:3–18.

14. Liou HL, Brennan NA. Anatomically accurate, finite model eye for optical modeling. _J Opt Soc Am A Opt Image Sci Vis_. 1997;14:1684–1695.

15. Kuszak JR, Zoltoski RK, Tiedemann CE. Development of lens sutures. _Int J Dev Biol_. 2004;48:889–902.

16. Gullstrand A. _Das brechende System des Auges [Germany]_. Hamburg-Leipzig: Verlag von Leopold Voss; 1909;299–306.

17. Gullstrand A. _How I Found the Mechanism of Intracapsular Accommodation_. Amsterdam: Elsevier Publishing Company; 1911;414–431.

18. Le Grand Y. _Form and SpaceVision_. Bloomington: Indiana University Press; 1967;133.

19. El Hage SG, Le Grand Y. _Optics of the Eye_. Berlin, Heidelberg: Springer-Verlag; 1980;57–69.

20. Shaker LM, Al-Adili A, AA Al-Amiery. Human eye response to the iris diameter variation at polychromatic light programmatically. _Journal of Physics: Conference Series_. 2021;1795:012025.

21. Piers PA, Norrby NE, Mester U. Eye models for the prediction of contrast vision in patients with new intraocular lens designs. _Opt Lett_. 2004;29:733–735.

22. Felipe A, Pastor F, Artigas JM, Diez-Ajenjo A, Gene A, Menezo JL. Correlation between optics quality of multifocal intraocular lenses and visual acuity: tolerance to modulation transfer function decay. _J Cataract Refract Surg_. 2010;36:557–562.

23. Poyales F, Garzon N. Comparison of 3-month visual outcomes of a spherical and a toric trifocal intraocular lens. _J Cataract Refract Surg_. 2019;45:135–145.

24. Smith G, Atchison DA. The gradient index and spherical aberration of the lens of the human eye. _Ophthalmic Physiol Opt_. 2001;21:317–326.

25. Smith G. The optical properties of the crystalline lens and their significance. _Clin Exp Optom_. 2003;86:3–18.

26. Kasthurirangan S, Markwell EL, Atchison DA, Pope JM. In vivo study of changes in refractive index distribution in the human crystalline lens with age and accommodation. _Invest Ophthalmol Vis Sci_. 2008;49:2531–2540.

27. Pope JM, Atchison DA. Measuring refractive index distribution in the human eye lens. _Oncotarget_. 2015;6:39395.

28. Brown NA, Vrensen G, Shun-Shin GA, Willekens B. Lamellar separation in the human lens: the case for fibre folds. A combined in vivo and electron microscopy study. *Eye (Lond)*. 1989;3(Pt 5):597–605.

29. Deane JS, Hall AB, Thompson JR, Rosenthal AR. Prevalence of lenticular abnormalities in a population-based study: Oxford Clinical Cataract Grading in the Melton Eye Study. *Ophthalmic Epidemiol*. 1997;4:195–206.

30. Frost NA, Sparrow JM, Moore L. Associations of human crystalline lens retrodots and waterclefts with visual impairment: an observational study. *Invest Ophthalmol Vis Sci*. 2002;43:2105–2109.

31. Qu J, Sasaki H, Fujisawa A, et al. Prevalence of lens opacity types except three major ones in Monzen Eye Study [Japanese]. *Rinsho Ganka (Jpn J Clin Ophthalmol)*. 2005;59:903–906.